BBAA VI International Colloquium on:
Bluff Bodies Aerodynamics & Applications
Milano, Italy, July, 20-24 2008

DOWNWIND SAILS AERODYNAMIC ANALYSIS

Ignazio Maria Viola[*] and Fabio Fossati[†]

[*] Dipartimento di Ingegneria Meccanica
Politecnico di Milano, Campus Bovisa, Via La Masa 34, 20156 Milano, Italy
e-mail: ignazio.viola@tiscali.it,

[†]CIRIVE Wind Tunnel
Politecnico di Milano, Campus Bovisa, Via La Masa 34, 20156 Milano, Italy
e-mail: fabio.fossati@polimi.it.

Keywords: Downwind Sail, Sailing Yacht, CFD, Wind Tunnel, Experimental Benchmark.

Abstract. *RANS code has been applied to an America's Cup Class Yacht to investigate sailing performance in downwind configuration. Apparent wind angles at 45°, 105° and 120° are reported, sailed with mainsail and asymmetrical spinnakers. Numerical results are in good agreement with wind tunnel data. A large mesh investigation have been performed, ranging from 60.000 elements up to 37 million elements, which shows a converging trend to the experimental values with differences smaller than 3% in both lift and drag. The most commonly used turbulence models in sails applications have been tested and the results are presented here in two meshes with 1 million elements and 6.5 millions, respectively. All models overestimates forces more than solving the Navier-Stokes system without any additional equations, hence turbulence models do not increase solution accuracy according to these results.*

1 INTRODUCTION

Present work has been carried out in a wider Ph.D. research project with the aim to set up a CFD tool to investigate the aerodynamic of an America's Cup Yacht. Since nineties the exponential increasing of the available computational resources motivate all the America's Cup (AC) challengers to investigate the ability of a Navier-Stokes solver to compute marine fluid dynamics problems and to substitute in-viscid code that were largely used since sixties. In the last two AC editions, Politecnico di Milano Wind Tunnel has conduct wind tunnel tests for *Prada Challenger* in the 31st AC and for *Lunarossa Challenger* in the 32nd AC, respectively. In 2004 Lunarossa has financed the Ph.D. grant with the aim to take advantage of the large amount of experimental data available from wind tunnel tests. Several sail-plans have been numerically investigated and a good agreement between experimentally measured and numerically computed global forces has been achieved. Therefore CFD has become a useful design tool, in particular to investigate the flow field with the visualization capabilities of the numerical computation and generally to improve the understanding of sail aerodynamics. In the present work are summarized the main achievements about downwind sails and three configurations are described, at 45°, 105° and 120° apparent wind angles respectively to include the most downwind sailed conditions in the last AC.

At closer yaw angles, id est in upwind conditions, the flow is mainly attached therefore non viscous codes can well predict aerodynamic forces. On the opposite, at larger angles, the flow is mainly separated on sail perimeters; hence global forces are less responsive to computational parameters. In the yaw angle range investigated, both separated and attached flow region have a strong influence in force production, lift is about twice drag force and none of them might be negligible. The flow around the spinnaker presents a turbulent cavitation nucleus along the luff (i.e. leading edge), where a secondary laminar cavitation nucleus (difficult to be detected) plays an important role in the first nucleus dimension [13]. Normally the discretization adopted does not permit to see neither the first nucleus. The reattached flow presents an accelerated boundary layer velocity profiles that is hard to catch with a standard computational wall function. Finally there is a leach (i.e. trailing edge) separation strongly connected to the tip vortex generated at the skirt (i.e. root) and at the head (i.e. tip) of the sail. The flow around the mainsail might be fully attached or separated. Moreover, at higher apparent wind angles, spinnaker is affected by alteration in the shape due to vortex shedding and consequently the separation points move along the chord. The studied phenomena presents most of the current challenge for computational fluid dynamics: transition, reattachment, relaminarization, both laminar and turbolent separations. Pressure measurements on sails and flow field visualization will allow in the future to compare CFD local results with experimental data, but at the present time only global forces are available.

In the following, the terminology presented in figure 1 will be adopted. The X and Y-axes are respectively trust and side direction with respect to the longitudinal axes of the yacht model, ignoring leeway angle. Aerodynamic force include forces acting on every part of the yacht above water-plane, hence windage effects are not subtracted. The horizontal components are generally decrypted as trust and side components, or drag and lift, where drag is aligned with the reference wind direction and lift is perpendicular to wind. The vertical component, i.e. along Z-axis, will not be discussed in the present work. Incoming flow has a vertical velocity gradient and a vertical twist [24], hence a reference height at 10m full-scale has been adopted to define a reference wind speed and wind direction. Apparent wind angle (AWA) is defined as the angle between the drag axis and the X-axis. Force components are expressed in terms of non-dimensional coefficients defined as follow:

$$CD = \frac{drag}{.5\rho V^2 S};\ CL = \frac{lift}{.5\rho V^2 S};\ CX = \frac{trustForce}{.5\rho V^2 S};\ CY = \frac{sideForce}{.5\rho V^2 S} \quad (1)$$

where ρ is density, V and S respectively reference wind speed and sail area.

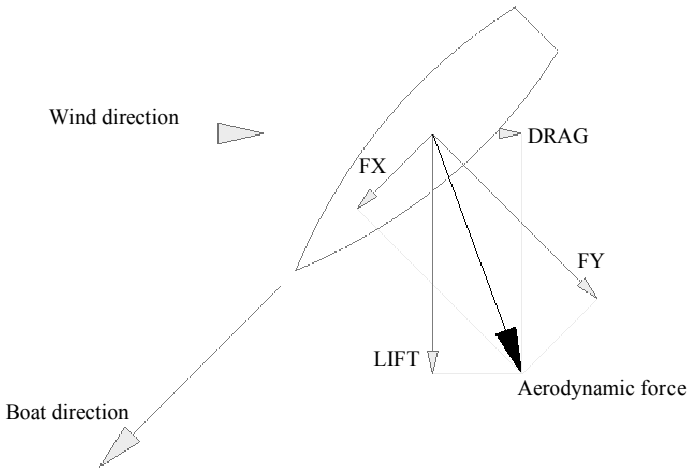

Figure 1: terminology, wind direction (hence drag and lift axis) is defined at the reference height of 10m full-scale.

2 STATE OF THE ART

In the following a state of the art overview is presented with the aim to put in evidence the innovative approach of the present work, mainly due to the exponential growing of the computational resources and hence, of the CFD potential strategies and capabilities.

The first numerical simulations of sails have been conducted in the sixties with in-viscid codes at the Massachusetts Institute of Technology, where Milgram developed vortex lattices method and flat wakes to investigate upwind sails, whose work has been published in 1968 [1], [2]. A few years later, in 1971, Gentry working for the aerospace *Boeing Company* of Seattle was investigating the mainsail and jib interaction with a panel method plus boundary layer solutions [3]. This work has been reviewed and updated ten years later by himself in [4] and most of his applications in the America's Cup design have been described in [5].

In nineties the increasing computational resources available made numerical codes the main design tool in advanced sail design. The well-known *North Sails* designer Burns Fallow described the computed aided design process of the successful Team New Zealand challenge to the 1995 AC [6]. The challenge to the AC by the New Zealand Yacht Squadron gave a strong impulse in the aerodynamic of sailing yacht research at the University of Auckland. In 1993 Hedges reported in his M.Sc. thesis [7] the first downwind RANS application: he adopted a finite-volume RANS solver named *CFDS-FLOW3D* with a k-ε turbulence model described in the followed publication on the Journal of Wind Engineering and Industrial Aerodynamics [8]. A structured mesh of hexahedral elements was applied because of the reduced computational capabilities in 1993, the spinnaker was decrypted by less then 400 elements against the on average over 200.000 elements of the present work. Hedges compared computed global coefficients with wind tunnel forces measured at 90° AWA. He tested several boom and pole angles to maximize trust force achieving a maximum lift (aligned with

trust axis at 90° AWA) 15% lower than the experimental data, and with 3% difference between numerical and experimental drag. The comparison did not include the hull, therefore at 90° AWA the flow field was mainly attached and a poor mesh and turbulence model could work adequately.

The second RANS application was performed by Miyata & Lee at the Tokyo University in 1999 onto an upwind configuration with an in-house-code and Baldwin-Lomax turbulence model [9]. The mesh was still structured hexahedral and it is non-conformal along a surface between main and jib to save grid points and to do not stretch the cells in between. They performed a conformal mesh to compare results and no significant differences have been reported. Computed trust force coefficient CX is over-estimated of less than 28% and side force coefficient CY is under-estimated of less than 18% compared to wind tunnel data for every tested AWA between 15° and 35°.

More recently, Collie have performed a large investigation upon the turbulence model for sail application, mainly based on 2D simulation. In 2001 Collie et al. [10] wrote a review of the turbulence models to be used in sail flow analysis, reporting comments and a detailed ranking for: k-ε (simply named ke in the following), k-ε with low-Re correction, k-ω in the original formulation, k-ω modified by Wilcox in 1998 (kw in the following), k-ω Shear Stress Transport (sst), k-τ, Spallart-Almaras (sa), Algebric-Stress-Model. The authors concluded that Spallart-Almaras model better perform in upwind condition and k-ω Shear Stress Transport in downwind condition. In [11] Collie et al. performed a 2D unsteady computations (URANS) with the CFD code Fluent testing the implemented models k-ε: in the original formulation (ke), in the formulation described by the Re-Normalization-Group (rng) and the more recent formulation named realizable (rlz). Benchmarks were primary performed on the backward facing step problem with a structured hexahedral mesh and y+ about 20 in the near-wall-region. The more recent rlz model performed better then the older and, hence, the authors supposed that it was adequate to simulate upwind conditions. A similar turbulence model test was performed with the code *CFX* and the implemented models ke, kw and sst, testing a spinnaker horizontal section [11]. The mesh was similar: structured hexahedral and y+ about 1 in the near-wall-region. The sst model better follow the experimental coefficient trends with the AWA and, hence, the authors supposed it was adequate to simulate downwind condition. In both Fluent and *CFX* tests, 2D formulations did not accurately modeled 3D flow thus numerical/experimental absolute global-forces differences were quite relevant. In 2006 Collie and Gerritsen [13] carried out another 2D computation about experiments on flat plate at low angle of incidence performed by Crompton in 2000 [14]. With a similar mesh and y+ smaller than 1, kw and sst model were compared and sst confirmed to perform better than kw. In this case the numerical/experimental comparison showed a very good agreement both on global forces and on of local measurements.

The first downwind RANS computation with tetrahedra has been published in 2003 by Richter, Horrigan and J.B. Brown [15]. To have a smaller mesh size in the near-wall-region they performed a local refinement. This work presented an innovative aero-elastic coupling between the CFD code *Fluent* (*Ansys Inc*) and the FE code *MemBrain* (*North Sails Inc.*) and no experimental comparison was presented.

In the last two years several authors have published a numerical/experimental comparison onto upwind configurations: Yoo & Kim [16, 17] with a structured mesh of 1.7M (millions)

cells and y+<50 obtained differences between numerical and experimental values lower than 83% in lift and 59% in drag; Ciortan & Soares [18] with 1M of tetrahedra and prismatic layers to reach 135<y+<270 showed differences lower than 86% in lift and 50% in drag; Querard & Wilson [19] with 2.4M of hexahedra and y+=O(10) obtained differences lower than 12% in lift and 24% in drag; Masuyama et al. [20] with a structured mesh of 0.5M hexahedra and y+=O(1) published qualitative differences in agreement, Viola [21] with 1.5M of tetrahedra and prismatic layers to reach y+=O(1) obtained differences lower than 3% in lift with a systematic over-estimation and 6% in drag.

About downwind configurations, RANS analysis have been reported in 2007 by Lasher & Richards [22] and in 2008 by Lasher & Sonnenmeier [23]. In the second work, authors tested 12 spinnakers and 6 turbulence models (ke, rlz, rng, kw, sst, rsm), with .33M and .14M of tetrahedra and 30<y+<120, obtaining averaged differences with wind tunnel data between 11% and 7% in lift and between 12% and 5% in drag. Authors focused onto turbulence model differences and tested only two (similar) meshes that returned relative differences about 5%.

In the present work three different downwind AWAs are simulated and compared, each with a 6M element mesh. The Numerical/Experimental ratios of the coefficients are anyway smaller than 8% for both lift and drag. A large investigation on the dependence of the solution from mesh size and topology is also presented. In particular, meshes up to 37M elements (larger more than 100 times any mesh founded in the reference, for downwind condition) have been tested. These exibit a converging trend towards the experimental values (differences smaller than 3% in lift and 2% in drag). Furthermore turbulence model, sa, ke, rlz, and sst, have been tested on two meshes, 1M elements with y+=O(30) and 6.5M elements with y+=O(10), respectively. All turbulence models over-predict the forces and increase the problem complexity without appreciable amelioration in solution accuracy.

3 WIND TUNNEL TESTS

Wind tunnel test have been performed at the Politecnico di Milano Twisted Flow Wind Tunnel in the boundary layer test sections. More details about the test section and the flow quality are published in [24]. Special devices to twist the incoming flow and modeling the changes in the apparent wind speed with the height have been adopted. More details about the Twisted Vanes Device can be found in [25].

The model scale is 1:12,5 to have the larger model without an excessive blockage effect. Model height is h=2.7m. Because the wind tunnel test section is 4m height and 14m wide, and a typical AC class sailing area is 800m^2, the blockage of the model is almost 0.1.

Model yacht drum type sheet are operated through a 7 channel proportional radio control system, except that the aerial is replaced by a hard wire link and the usual joystick transmitter is replaced by a console with a 7 multi turn control knobs that allow winch drum positions to be recorded an re-established if necessary. The sail trimmer, who operates from the wind tunnel control room, controls the sheet trims. A six components balance is placed inside the yacht hull. The data acquisition software calculates the forces and moments using the dynamometer calibration matrix. The forces are shown in the virtual panel designed on the computer screen in real time so that the sail trim can be optimized, because the effects of trimming the sails on the driving and heeling forces can be directly appreciated.

Figure 2 shows a standard test at 45° AWA. Back to the model, the Twisted Vanes Device might be appreciated and also the wide extension of the test section (about 40m long) which

allows the boundary layer generation. More details about the test procedure are published in [24]

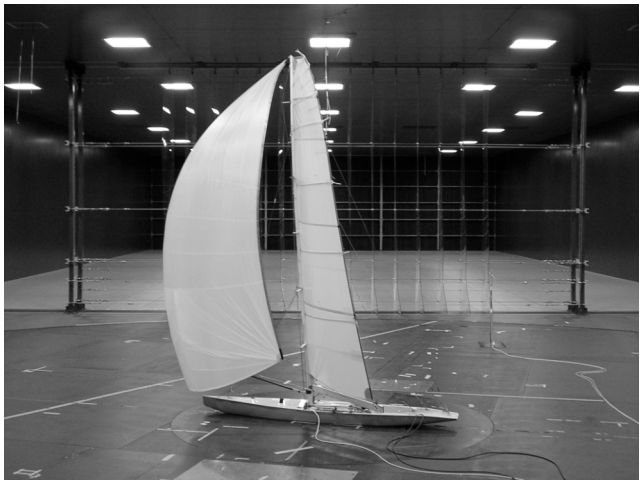

Figure 2: Lunarossa model scale in the boundary layer test section of the Politecnico di Milano Twisted Flow Wind Tunnel sailing at 45° AWA.

Immediately after the force measurements, an operator goes inside the wind tunnel and takes pictures with a high-resolution camera. With a devoted software, images are collected together and a three dimensional mathematic flying shape is reconstructed.

Three sail-plan configurations are reported at three AWAs: 45°, 105° and 120°. Nominal apparent wind angle AWA is defined as the angle between the boat longitudinal axis and the undisturbed incoming apparent wind at 10m height from the water plane which coincides with wind tunnel longitudinal axes. Two asymmetric spinnakers have been considered, A1 and A4, where identification number increase with the design apparent wind angle range. Hence A1 has been sailed at 45° AWA and A4 at 105° and 120° AWA. The same mainsail A2 has been sailed at every angles.

Mainsails are built with horizontal mylar panels and asymmetric spinnakers with tri-radial polyester panels, hence in similar materials than in full-scale but with smaller thickness. The asymmetrics would be able to fly in a similar manner than in full-scale if a the Froude number based on the material thickness t is conserved:

$$Fr = \frac{V}{\sqrt{g \cdot t}} \tag{2}$$

where V is nominal wind speed, g gravity acceleration, t thickness .

For this reason wind tunnel wind speed changes with the asymmetric spinnakers tested and the corresponding full scale wind speed.

In figure 3 the experimental lift and drag coefficients and the centre of effort height are plotted versus apparent wind angle. A more detailed grid cannot be presented because data are confidential. The three reported sail trims correspond to the optimum trims that maximize the trust components along the boat direction for each AWA. The lift corresponds to the trust component when sailing at AWA 90°, hence it has always a positive components in the trust direction. On the opposite, at 45° the drag has a negative component in trust direction and at AWA greater than 90° it has a positive component. Experimental values show that increasing the apparent wind angle, the lift always decreases and the drag is maximum at 105°.

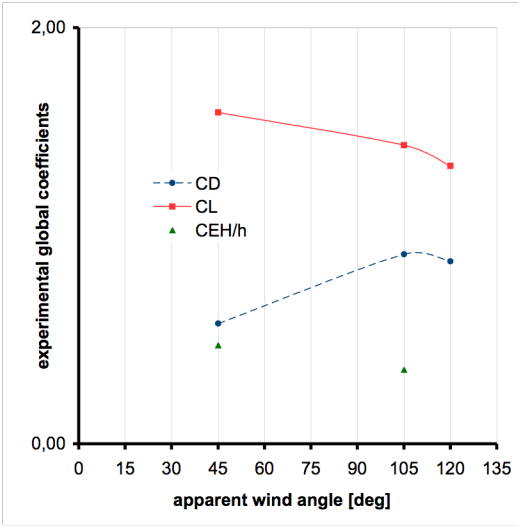

Figure 3:experimental lift CL and drag CD coefficient, and centre of effort height CEH normalized on model height h, measured at 45°, 105° and 120° AWA.

4 NUMERICAL SETUP

Navier-Stokes equations have been solved with RANS technique. Sail Aerodynamics might be considered a relative high Reynolds number ($4 \cdot 10^5$, computed on the model height h) and low Mach number ($7 \cdot 10^{-3}$) dynamics, hence density variation can be neglected, energy conservation equation leaves unresolved, and Navier-Stokes equations might be presented as:

$$\vec{\nabla} \cdot \vec{u}^* = 0$$
$$\left(\vec{u}^* \cdot \vec{\nabla}\right)\vec{u}^* = -\vec{\nabla} p^* - \frac{1}{\mathrm{Re}} \nabla^2 \vec{u}^* \qquad (3)$$

where u* and p* are respectively non dimensional velocity and pressure, Re is the Reynolds number.

In equation (3) it can be observed that the only scale index is presented by the Reynolds number, hence it must be the same in numerical computation and experimental test. The full-scale Reynolds number is almost 10 times larger but it is usually unreachable in wind tunnel test because of fragility of the model scale.

The flow field around the sail is mainly turbolent and a number of grid points of the order of $\mathrm{Re}^{9/4} = 4 \cdot 10^{11.5}$ might be used to compute all the turbulence scale from the larger one that input energy to the smaller one that pull out energy for viscous dissipation. In the present work a number of cells up to $4 \cdot 10^7$ have been reached, therefore turbulence models have been tested to verify if any additional enhancement would have been achieved taking into account the grid-filtered small-scale effect into the averaged flow field. Additional turbulence model equations have not returned significant advantages as reported in paragraph 7.

Computed global forces are compared with measured forces in terms of non-dimensional coefficients of drag and lift components or trust and side force components:

Force components perpendicular to the horizontal plane are much less meaningful and have been neglected in the present publication.

Center of effort height CEH is reported vertically from the water plane and it is divided by the boats model height h. It is computed dividing heeling moment to side force.

The commercial preprocessors *Gambit v2.4.6* and *Tgrid v5.0.6* (*Ansys Inc.*) have been used to build a tetrahedral mesh with a bottom-up approach. Different mesh size have been performed from 60.000 to 37.000.000 cells and observed differences will be discussed in paragraph 6. No prism layers have been used and averaged y+ from 50 to 5 have been reached.

Fluent v6.3.26 (*Ansys Inc.*) has been adopted in the implicit pressure-based steady formulation, with a SIMPLE scheme and first order discretization. Inlet and outlet boundary condition have been posted respectively 5h windward and 10h leeward the model, and the wind tunnel cross section has been tightened to avoid the modeling wall velocity profile, hence slip-condition have been imposed on the water plane, at 3h on both sides and at 0.3h over the top of the model.

5 NUMERICAL RESULTS

In figure 4 the three sail trims are presented and the corresponding aerodynamic force is plotted. The force vector is scaled and oriented for the three AWAs. The sails are always in a similar position respecting wind direction that comes horizontally from left in each sketch, however increasing AWA the boat direction changes and the asymmetric is trimmed to obtain a deeper horizontal shape. The figure shows that the order of magnitude and the direction of the aerodynamic force is similar for each AWA but the projection on the boat coarse changes significantly. Despite of this, the flow field changes appreciably as it will be showed in the following.

In the table below (table 1) the numerical/experimental coefficient ratios are presented for the lift and drag components and for the three AWAs. Numerical results are in good agreement with experimental data. The differences are always less than 8%**.**

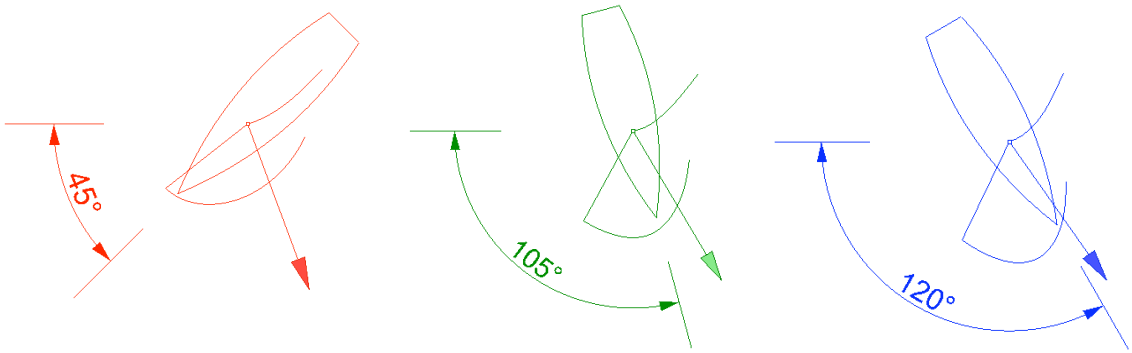

Figure 4: apparent wind angle, boat direction, sail position and resultant aerodynamic force vector are sketched for the three reported conditions.

AWA	**45°**	**105°**	**120°**
$CD^{num/exp}$	1.02	1.00	1.08
$CL^{num/exp}$	0.97	1.08	1.00

Table 1: Numerical/experimental lift and drag ratios for the three reported conditions.

Figure 5 shows asymmetric spinnaker flying shapes are shown from the drag axis (leeward perspective) and pressure coefficient distribution is plotted respectively for 45°, 105° and

120° AWA. Red regions mean high pressure and blue region means lower pressure as indicated in the color bar on the left. Black lines show iso-pressure value: Cp=.5, 0, -.5, -1, -2 and two horizontal lines indicate the $^1/_3$h and $^2/_3$h reference heights for the following figures. Pressure coefficient is defined as follow:

$$Cp = \frac{p - p_0}{.5\rho V^2}; \tag{4}$$

where p is the local static pressure, p_0 the reference pressure on the outflow boundary, ρ the density and V the reference wind speed.

The figure shows the flying shapes exposition to the wind and the vertical position of the minimum pressure region changing with the increasing AWA-

Figures 6, 7 and 8 show non-dimensional dynamic pressure coefficient q* distribution onto $^1/_3$h (left) and $^2/_3$h (right) reference heights, respectively for 45°, 105° and 120° AWA. Red regions show high speed areas and blue regions are low speed areas with reference to the respective color bar. Lines are iso-pressure values: Cp=.5, 0, -,5, -1 and -2. Dynamic pressure coefficient q* is defined as follow:

$$q^* = \frac{u^2}{V^2} \tag{5}$$

where u is the local velocity and V the reference velocity.

The figures show flying shape horizontal sections changing with the increasing AWA: sections become deeper and the differences between upper sections and lower sections increase. Low speed region (dark blue) on leeward side of sails indicates separated flow. The flow is separated in the higher sections at 45° AWA and attached in the lower sections. At 105° AWA the vice versa occurs, the lower sections are deeper than the higher ones. At 120° AWA the flow is still attached only in a small region on the leeward side of the asymmetric and the flow on the leeward side of the mainsail is fully separated.

Figures 9, 10 and 11 show Cp curves onto $^1/_3$h (left) and $^2/_3$h (right) reference heights respectively for 45°, 105° and 120° AWA. Curves are plotted versus adimensional chord length. Blue curve and red curve show respectively asymmetric spinnaker and mainsail Cp. In figure 9, on the left, blue line shows a typical pressure distribution for a high cambered profile: pressure decrease on leeward side of the asymmetric up to about 30% of chord line, then both pressure and its adverse gradient increase until separation occurs and pressure becomes constant. On the windward side, pressure coefficient increase up to one where local static overpressure ($p - p_0$) is equal to the inflow dynamic pressure ($.5\rho V^2$).

When the flow is fully separated, the pressure profile is almost constant along the chord.

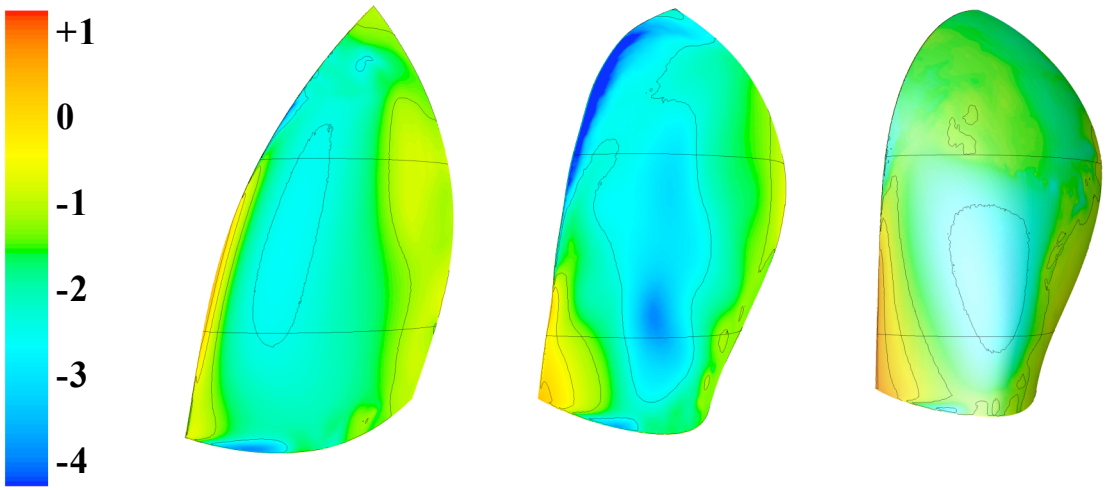

Figure 5: contours of pressure coefficient on leeward side of the asymmetrics at 45°, 105 and 120° AWA respectively; iso-pressure values are tracked for Cp=.5, 0, -.5, -1, -2.

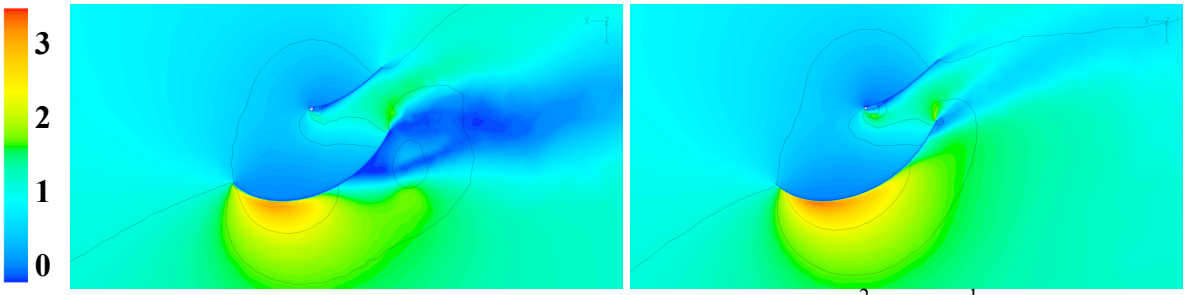

Figure 6: adimensional dynamic pressure contours at 45° AWA for $^{2}/_{3}$h and $^{1}/_{3}$h respectively, isopressure values are tracked for Cp=.5, 0, -,5, -1, -2.

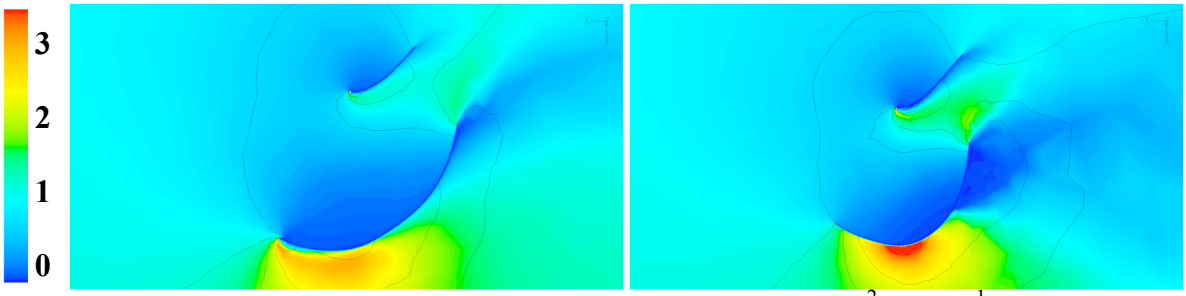

Figure 7: adimensional dynamic pressure contours at 105° AWA for $^{2}/_{3}$h and $^{1}/_{3}$h respectively, isopressure values are tracked for Cp=.5, 0, -,5, -1, -2.

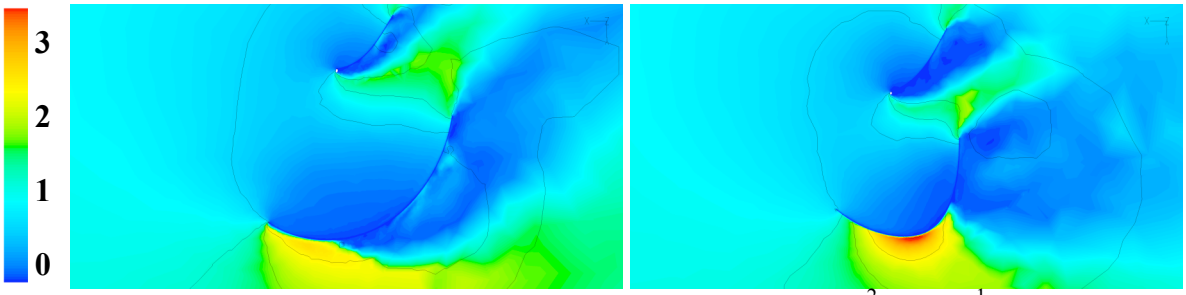

Figure 8: adimensional dynamic pressure contours at 120° AWA for $^{2}/_{3}$h and $^{1}/_{3}$h respectively, isopressure values are tracked for Cp=.5, 0, -,5, -1, -2.

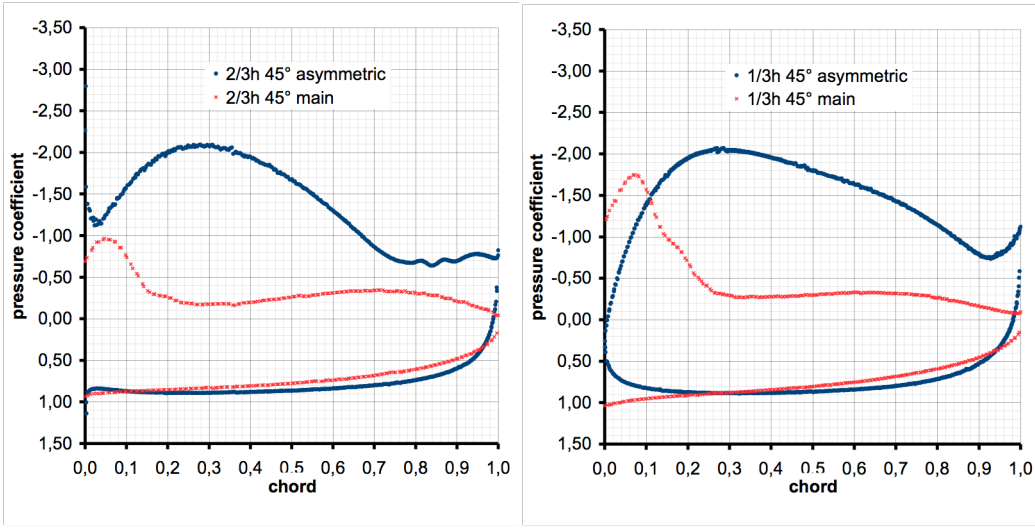

Figure 9: pressure coefficients along sail chords of mainsail and asymmetric at 45° AWA for $^{2}/_{3}$h and $^{1}/_{3}$h, respectively.

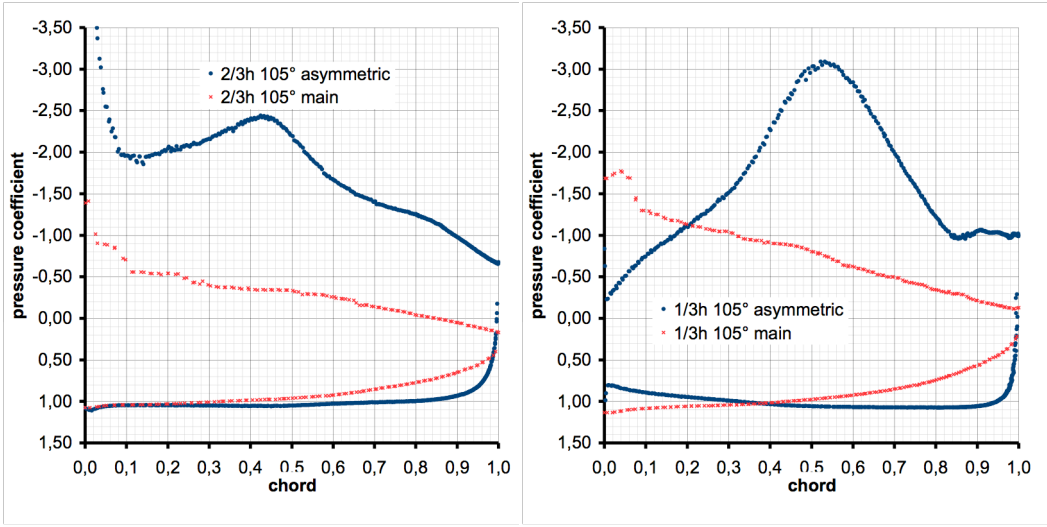

Figure 10: pressure coefficients along sail chords of mainsail and asymmetric at 105° AWA for $^{2}/_{3}$h and $^{1}/_{3}$h, respectively.

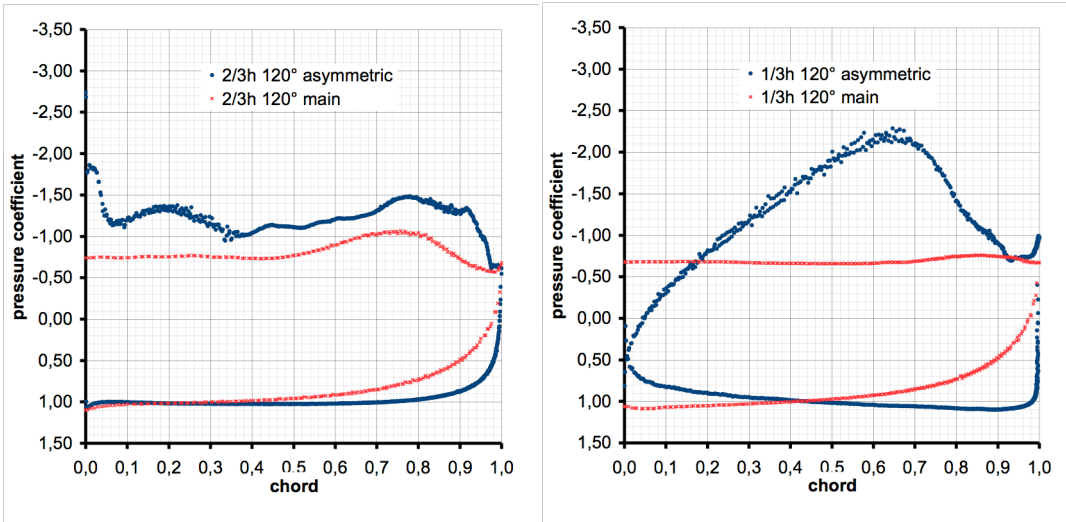

Figure 11: pressure coefficients along sail chords of mainsail and asymmetric at 120° AWA for $^{2}/_{3}$h and $^{1}/_{3}$h, respectively.

6 MESH SENSITIVITY INVESTIGATION

In the present work an AMD Opteron 275 dual core with 74 nodes at 2.2 GHz each with 2GB RAM allows to perform large fully tetrahedral meshes. Four similar meshes has been built for the 45° AWA configuration.

Figure 12 shows computed lift and drag coefficients divided by the experimental value for the four meshes at 45° AWA. None turbulence model has been adopted. The figure shows that increasing the number of cells from 60.000 to 36 millions, the coefficients seems to converge to the experimental value: differences between computed and experimentally measured global coefficients are more than 5% with 1M elements and smaller than 3% with 37M elements. Figure 13 shows y+ decreasing trend computed onto the asymmetric horizontal section at 1/3h, y+ computed as follow:

$$y^+ = y \cdot \frac{1}{\nu}\sqrt{\frac{\tau_w}{\rho}}; \tag{6}$$

where y is first cell-centre-height from the wall, ν viscosity, ρ density, τ_w wall shear stress.

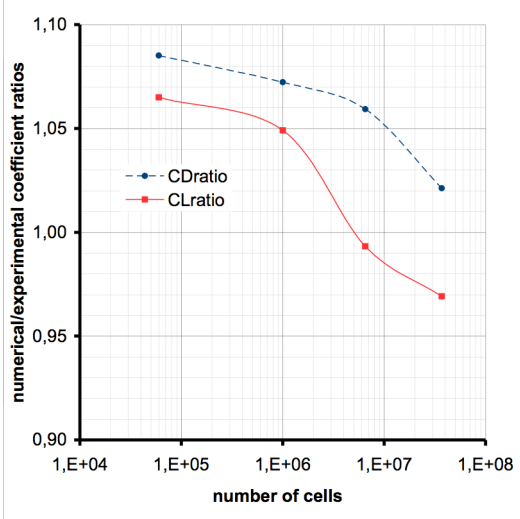

Figure 12

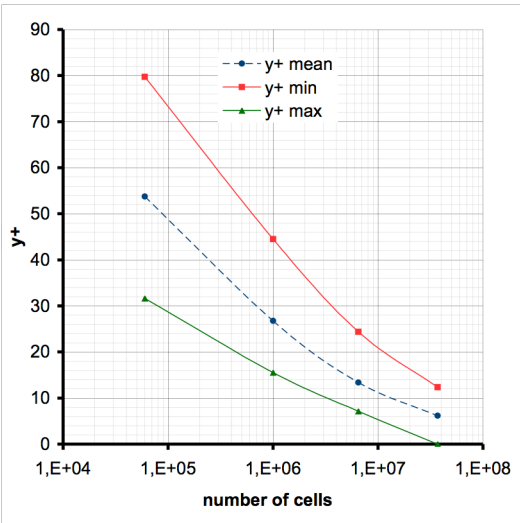

Figure 13

Meshes have similar grow rate about 1.2 (the ratio between the linear dimension of two adjacent cells in a wall normal direction) and similar maximum element size, hence decreasing the element size in the near-wall-region; there is decrease in both first cell-centre-height and y+ , while there is an increase in overall number of elements and also the degree of freedom to be solved and the computational effort increase. This approach allows to built several meshes topologically identical but with an increasing space resolution. It is a computationally expensive approach but it permits to investigate the effect of the space resolution when it is not know a priori where the lack of resolution mostly affects the computed solution. In fact, tetrahedral elements, soft grow rate about 1.2, without refinements and non-conformal faces, allow to minimize the mesh influence onto the solution but, on the other hand, lead to an expensive grow of the number of elements to solve the near-wall-region gradients. In particular, y+=O(30) with meshes of the order of 1M cells, as adopted in the most recent works [22, 23]. In this work 37M elements have been used to reach y+=O(5). To obtain smaller y+ values without increasing the number of elements, many authors have adopted hexahedral or prismatic elements. In fact hexahedra and prism elements generate structured grid which could be compressed along one dimension, hence, they allow to refine the gradient discretization along one direction without increasing excessively the overall number of mesh elements. On the

other hand, stretched hexahedra or prisms, determine an anisotropic behavior of the discrete derivative operator hence they might induce an anisotropic derivative field. It is well-known that linear system solver techniques perform more efficiently onto an equally spaced grid in all directions [26]. As an example, Figure 14 shows non-dimensional vorticity contours on a horizontal section at 1/3 of the height of a model sailing in upwind condition, computed with tetrahedral elements and with prismatic elements respectively. The two sail sections, the jib one and the main one, present on leeward side a high vorticity region showed in red: on the left tetrahedra allow an isotropic derivate operator and, on the right, prisms lead to an anisotropic velocity gradient computation. More details about simulation reported in figure 14 might be found in [21].

Another aspect that might be considered is the transition from the prism region to the tetrahedral region when both the element types are adopted, as performed in [18]. As an example, the same upwind geometry presented in figure 14 has been meshed with tetrahedral elements except for the near-wall-region where 10 prismatic layers have been adopted. In figure 15 and 16 two different meshes have been performed with the same grow rate, but the first prism layer height in figure 15 is half of that showed in figure 16. The two mesh schemes are presented in figures. The transition from the prismatic region to the tetrahedral region in the case with the lowest prismatic height is more abruptly than in the case with the highest prismatic height. As a consequence, the two regions do not correctly communicate each other and the separation occurs inside the prismatic region but do not propagate into the tetrahedral region. Figure 16 shows the velocity vector field with the low prismatic region: the thin sail presence generate a velocity profile that separates on the leeward side but separation occurs only in the prismatic region and it does not affect the tetrahedral region. In figure 17 the same location along the sail is presented but meshed with a higher prismatic region: the velocity profile inverts both in the prismatic region and in the tetrahedral region.

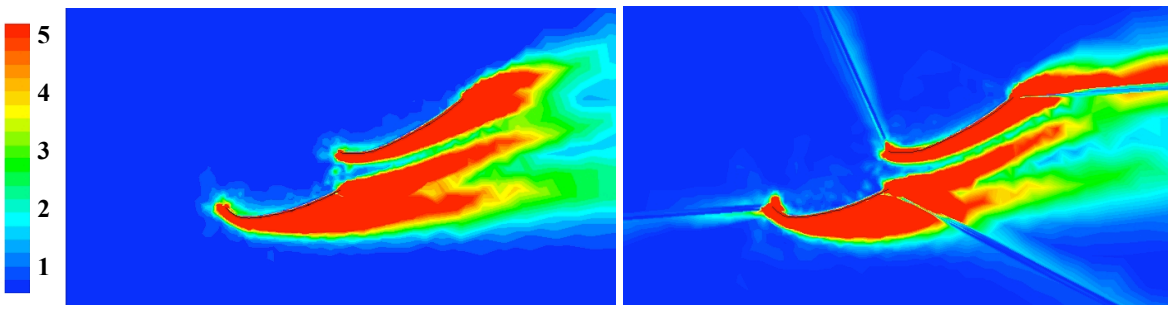

figure 14: voticity contours on an horizontal section in upwind condition computed with tetrahedral elements (left) and prismatic elements (right), showing the anisotropic behavior of the derivative operator.

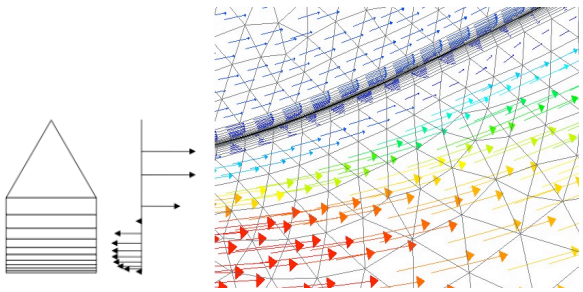

Figure 15

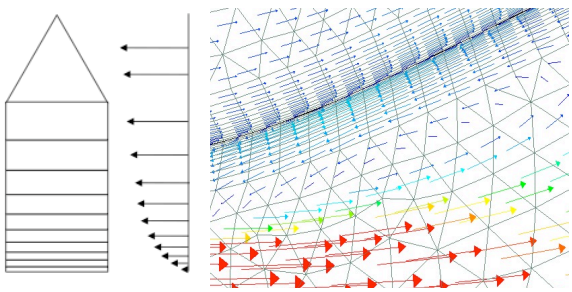

Figure 16

7 TURBULENCE MODELS

To perform a Direct-Navier-Stokes computation, it should be used a number of cells of the order of one tera-elements but at present day it is still unaffordable. Therefore, turbulence models could be used to take into account the grid filtered fluctuations effect on the averaged flow field. Models require one (e.g. sa) or two (e.g. ke and kw) additional equations to be solved and most of the formulations are not able to relax turbulent quantities when the flow speed is significantly reduced in the near-wall-region (namely low-Reynolds correction). Hence, wall-functions have to be implemented adding new equations to be solved. On the other hand, turbulence models are far from being universal models applicable to any flow condition and wall functions are well known to work un-properly with separated flow, so several corrections could be implemented to let them model separated boundary layers. Therefore, turbulence models should be applied only if a significant accuracy increase is achieved or to increase stability in fluctuating solutions. The following results will show that against the increasing complexity and arbitrary in the equation system to be solved, turbulence models do not increase significantly accuracy.

At the current state of the art, turbulence models have been tested with large y+ and hence with wall functions. Therefore in the present work the Fluent implemented *non-equilibrium* wall function has been adopted. Six turbulence models have been tested with two mesh: 1M elements with y+=O(30) and 6.5M elements with y+=O(15), respectively. The first cell-centre of the coarser mesh should be in the so called logarithmic layer and the cell-centre of the finer mesh should be in the buffer layer between the viscous sub-layer and the logarithmic layer.

The following models have been tested: sa, ke, rng, klz, kw, sst. Two thousands iterations have been performed for each of them starting from the solution obtained without any model. Each of them has converged to a new force value.

Figure 17 and 18 show drag and lift numerical/experimental coefficient ratios respectively, obtained without any models (named none in figure) and with the six models. The models are presented in order of predicted drag ratio values. All of them over-predict drag components more than computation without any model and it does not depends on mesh size. All models over-predict lift independently from mesh size again, but there is no congruence between drag and lift over-prediction order.

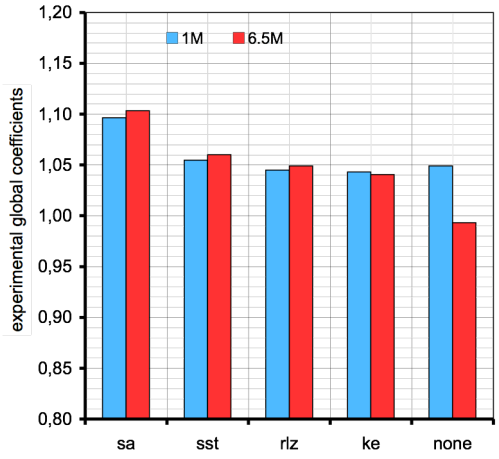

Figure 17

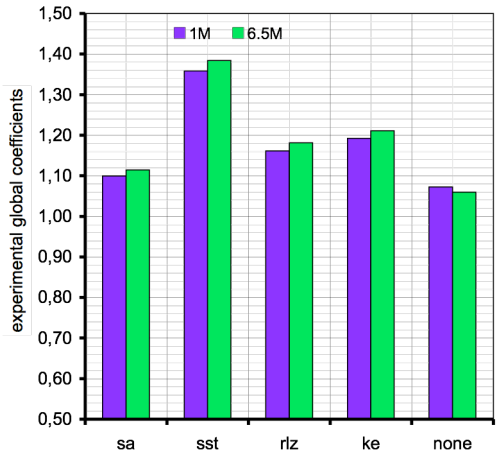

Figure 18

8 CONCLUSIONS

RANS code has been used to investigate the sail aerodynamics under downwind condition. The flow is mainly attached at 45° AWA on both mainsail and asymmetric spinnaker. Increasing the AWA to 105° and 120°, a large separated region is observed on both sails. The numerical/experimental differences on global force coefficients computed with about 6 million element meshes is smaller than 8% in both lift and drag components for each AWA. A large mesh investigation has been performed and meshes, ranging from 60.000 elements up to 37 millions, showing a converging trend to the experimental data with differences smaller than 3% in lift and 2% in drag. A mesh-independent solution has not yet been achieved, suggesting that a more detailed simulation is necessary in the next future.

Differently from the above referenced results, also the four more common turbulence models in sail applications have been tested on two meshes, with 1 million elements and 6.5 millions, respectively. All the turbulence models produced a systematic over-estimation of force components independently from mesh size. Hence, it seems that the increased computational complexity associated to a turbulence model has not lead to more accurate results in this work.

ACKNOWLEDGEMENTS

Authors would like to thanks sail designers Guido Cavalazzi, Henrik Soderlund, Grant Spanhake and yacht designer coordinator Claudio Maletto of Lunarossa 32nd AC Challenger to have always supported and believed in this research; Giuseppe Passoni and Raffaele Ponzini for their precious suggestions.

REFERENCES

[1] J.H. Milgram: *The Aeodynamic of Sails*; proceedings of 7th Symposium of Naval Hydrodynamic, pp. 1397-1434, 1968.

[2] J.H. Milgram: *The Analitical Design of Yacht Sails*; Trans. SNAME, pp. 118-160, 1968.

[3] A.E. Gentry: *The Aerodynamics of Sail Interaction*; The Ancient Interface III, 3rd AIAA Symposium on Sailing, Redondo Beach, California, US, Nov. 20, 1971.

[4] A.E. Gentry: *A Review of Modern Sail Theory*; The Ancient Interface XI, 11th AIAA Symposium on Sailing, Seattle, Washington, US, Sept. 12, 1981.

[5] Gentry A.E.: *The Application of Computational Fluid Dyamics to Sails*; proceedings of the Symposium on Hydrodynamic Performance Enhancement for Marine Applications, Oct. 31, Newport, Rhode Island, 1888.

[6] J. Burns Fallow; *America's Cup Sail Design*; Journal of Wind Engineering and Industrial Aerodynamics, **63** 183 192, 1996.

[7] K.L. Hedges: *Computer Modelling of Downwind Sails*; MF Thesis, University of Auckland, New Zealand, 1993.

[8] K.L. Hedges, P.J. Richards, G.D. Mallison: *Computer Modelling of Downwind Sails*; Journal of Wind Engineering and Industrial Aerodynamics **63** 95 110, 1996.

[9] H. Miyata, Y.W. Lee: *Application of CFD Simulation to the Design of Sails*; Journal of Marine Science and Technology, **4**:163-172, 1999.

[10] S.J. Collie, M. Gerritsen, P. Jackson; *A Review of Turbulence Modelling for Use in Sail Flow Analysis*; School of Engineering Report No. 603; Auckland, NZ, October 23, 2001;

[11] S. Collie, M. Gerritsen, M. O'Sullivan: *Numerical Simulation of the Turbulent Flow Past Upwind Yacht Sail*, Journal of Wind Engineering and Industrial Aerodynamics, Sept. 2002.

[12] S. Collie, P. Jackson, M. Gerritsen: *Validation of CFD Methods for Downwind Sail Design*; High Performance Yacht Design Conference, Auckland, New Zealand, Dec. 2002.

[13] S. Collie, M. Gerritsen: *The Challenging Turbulent Flows Past Downwind Yacht Sails and Practical Application of CFD to Them*; 2nd High Performance Yacht Design Conference, Auckland, February 2006

[14] M. Crompton, R. Barrett: *Investigation of the Separation Bubble Formed Behind the Sharp Leading Edge of a Flat Plate at Incidence*; Proceedings of the Institution of Mechanical Engineers, Part G, **214**, pp. 157 176, 2000.

[15] H.J. Richter, K.C. Horrigan, J.B. Braun: *Computational Fluid Dynamics for Downwind Sails*; The 16th Chesapeake Sailing Yacht Symposium, March 2003.

[16] J. Yoo, J. Kim, I. Park, H. Ahn, S. Van: *CFD Calculation on the Sail Like Three Dimensional Airfoils*; 2nd High Performance Yacht Design Conference, Auckland, Feb. 2006

[17] J. Yoo, H.T. Kim: *Computational and Experimental Study on Performance of Sail of a Sailing Yacht*, Ocean Engineering, **33**, 1322-1342, 2006.

[18] C. Ciortan, C.G. Soares: *Computational Study of Sail Performance in Upwind Condition*, Ocean Engineering, **34**, 2198-2206, 2007.

[19] A.B.G. Querard and P.A. Wilson; *Aerodynamic of Modern Square Head Sails: a Comparative Study Between Wind-Tunnel Experiments and RANS Simulations*; In the Modern Yacht, Southampton, UK, 11-12 Oct 2007. London, UK, The Royal Institution of Naval Architects, 8pp, 107-114, 2007. http://eprints.soton.ac.uk/49314/.

[20] Y. Masuyama, Y. Tahara, T. Fukasawa, N. Maeda: *Database of Sail Shapes vs. Sail Performance and Validation of Numerical Calculation for Upwind Condition*; The 18th Chesapeake Sailing Yacht Symposium, Annapolis, Maryland, USA, March 2007.

[21] I.M. Viola: *Numerical and Experimental Flow Dynamics applied to Sailing Yacht Dynamics*, Ph.D. Thesis, Politecnico di Milano, May 2008.

[22] W.C. Lasher, P.J. Richards: *Validation of RANS Simulations for International America's Cup Class Spinnaker Force Coefficients in an Atmospheric Boundary Layer*; J. Ship Res. 51 **1**, 22–38, 2007.

[23] W. Lasher & J. Sonnenmeier: *An Analysis of Practical RANS Simulations for Spinnaker aerodynamics*; Journal of Wind Engineering and Industrial Aerodynamics, **96** 143–165, 2008.

[24] F. Fossati, S. Muggisca, I.M. Viola, A. Zasso: *Wind Tunnel Techniques for Investigation and Optimization of Sailing Yachts Aerodynamics*; proceedings of the 2nd High Performance Yacht Design Conference; Auckland; Feb. 2006.

[25] A. Zasso, F. Fossati, I.M. Viola: *Twisted Flow Wind Tunnel Design for Testing Yacht Sails*; proceedings of EACWE4 European and African Conference on Wind Engineering, Praga (Rep. Ceca); July 2005.

[26] K. Stueben: *Introduction to Algebraic Multigrid:* In C. W. Oosterlee U. Trottenberg and A. Schuller, editors. Academic Press, New York, 2001.